Journal of Advanced Research (2013) 4, 501–508

Cairo University

Journal of Advanced Research

ORIGINAL ARTICLE

Multiproperty empirical isotropic interatomic potentials for CH_4–inert gas mixtures

M.S.A. El-Kader *

Department of Engineering Mathematics and Physics, Faculty of Engineering, Cairo University, Giza, Egypt
Department of Physics, Deanship of Preparatory Year, Shaqra University, Shaqra, Saudi Arabia.

Received 14 July 2012; revised 28 August 2012; accepted 28 August 2012
Available online 6 November 2012

KEYWORDS

Intermolecular potential;
Absorption;
Scattering;
CH_4–inert gases

Abstract An approximate empirical isotropic interatomic potentials for CH_4–inert gas mixtures are developed by simultaneously fitting the Exponential-Spline-Morse-Spline-van der Waals (ESMSV) potential form to viscosity, thermal conductivity, thermal diffusion factors, diffusion coefficient, interaction second pressure virial coefficient and scattering cross-section data. Quantum mechanical lineshapes of collision-induced absorption (CIA) at different temperatures for CH_4–He and at $T = 87$ K for CH_4–Ar are computed using theoretical values for overlap, octopole and hexadecapole mechanisms and interaction potential as input. Also, the quantum mechanical lineshapes of collision-induced light scattering (CILS) for the mixtures CH_4–Ar and CH_4–Xe at room temperature are calculated. The spectra of scattering consist essentially of an intense, purely translational component which includes scattering due to free pairs and bound dimers, and the other is due to the induced rotational scattering. These spectra have been interpreted by means of pair-polarizability terms, which arise from a long-range dipole-induced-dipole (DID) with small dispersion corrections and a short-range interaction mechanism involving higher-order dipole–quadrupole **A** and dipole–octopole **E** multipole polarizabilities. Good agreement between computed and experimental lineshapes of both absorption and scattering is obtained when the models of potential, interaction-induced dipole and polarizability components are used.

Introduction

In a previous work, we compared measurements of collision-induced absorption (CIA) and of collision induced light scattering (CILS) spectra of hydrogen, inert gas mixtures and CF_4–He gas mixtures with theoretical profiles that were based on the empirical induced dipole for CIA, induced trace and anisotropy polarizabilities for CILS, and new advanced interaction potential [1–4]. Due to the observed agreements for both spectra of absorption and scattering for these gas mixtures, we use the same treatment of transport, thermophysical properties

* Tel. +20 1282808985.
E-mail address: Mohamedsay68@hotmail.com
Peer review under responsibility of Cairo University.

Production and hosting by Elsevier

2090-1232 © 2012 Cairo University. Production and hosting by Elsevier B.V. All rights reserved.
http://dx.doi.org/10.1016/j.jare.2012.08.013

and scattering cross-sections data for CH_4–inert gas mixtures, to construct the parameters of the interaction potentials.

Collisional pairs of molecules in dense phase show an absorption band in the far infrared region of the spectrum [5,6]. This absorption is due to the induced dipole moment arising from the distortion of the electronic clouds during the collision of two molecules. As the induced dipole moment depends on the distance between the colliding pair, the translational state of the system can change due to the interaction of the induced dipole with the electromagnetic field, giving rise to a rototranslational absorption band. Measurements of collision-induced absorption (CIA) spectra give therefore information on interatomic interactions. Specifically, spectral lineshapes and intensities reflect certain details of the induced dipole as function of the interatomic separation and the collision dynamics (i.e. the interatomic potential).

On another level, the anisotropic collision-induced light scattered by a fluid and dense gases due to collisional interactions, has a power spectrum which is shaped by two functions of the interatomic separation r, the interatomic potential $V(r)$ and the anisotropy $\beta(r)$ of the induced polarizability [7,8]. Information on the molecular interactions may be obtained from this spectrum. For the lower-frequency part of collision-induced spectrum, the dipole-induced-dipole (DID) interaction and electron exchange contributions account for most of the observed scattering intensities, whereas, at high frequency range (the well region of the intermolecular potential), higher-order multipolar polarizabilities have to be taken into account and can thus be measured for molecular pair against the classical DID background [9]. For mixtures and molecular gases, the excess polarizability induced by interactions in a pair is a tensor that has anisotropy $\beta(r)$ related to the anisotropic collision-induced light scattering (CILS). Recently, we showed for a few characteristic systems that the spectral properties of anisotropic interaction-induced light scattering can be calculated for the gaseous state, on the basis of classical, empirical or *ab initio* models of the induced anisotropy and of the interaction potential [10–12].

As no adequate potentials are available for these mixtures, we calculate an approximate isotropic interatomic potential using mostly the methods outlined in a previous paper [4]. Since the details of the methods are given there and the references therein, we will only restate the equations when it is necessary for the sake of continuity. To reiterate, the basic strategy in this paper is to include collision-induced absorption and collision-induced light scattering data in addition to the data on second pressure virial coefficients, mixtures viscosity, diffusion, thermal conductivity coefficients and isotopic thermal factors to fit the simple functional form of the Exponential-Spline-Morse-Spline-van der Waals (ESMSV) interatomic potentials for CH_4–inert gas interactions.

The transport, thermophysical properties and scattering cross-section data used in the fitting are complementary ones for that purpose. For these mixtures, the viscosity, thermal conductivity, isotopic thermal factor and diffusion data are most sensitive to the wall of the potential from r_m inward to a point, where the potential is repulsive [13]. The second pressure virial coefficients reflect the size of r_m and the volume of the attractive well [14], while the integral scattering cross-section contains detailed information on the potential well features and long-range attraction [15].

Our paper is organized as follows. The adopted intermolecular potential model with the calculations of different properties are presented in Section 2. The analysis of collision-induced absorption (CIA) and light scattering (CILS) spectral moments to determine the parameters of the induced dipole and the anisotropy models is given in Section 3, with the results are presented and discussed in detailed and the concluding remarks are given in conclusion section.

The intermolecular potential models and multiproperty analysis

In order to calculate the line profiles of absorption and scattering and their associated moments, the intermolecular potential is needed. Results with different potentials can be compared with experiment to assess the quality of the potential.

The intermolecular potential we provide here is obtained through the analysis of a set of gaseous transport properties [16–19], the second pressure virial coefficients [19–24] and integral scattering cross-section [25].

For the analysis of all these experimental data we consider the Exponential-Spline-Morse-Spline-van der Waals (ESMSV) model [26].

$$V(r) = \varepsilon A_0(\exp(-B_0(r/r_m-1)) \quad 0 \leqslant r \leqslant r_1 \tag{1}$$

$$= \varepsilon\exp(a_1+(r/r_m-r_1/r_m)\{a_2+(r/r_m-r_2/r_m)[a_3 + (r/r_m-r_1/r_m)a_4]\}) \quad r_1 \leqslant r \leqslant r_2 \tag{2}$$

$$= \varepsilon\{\exp[-2\xi(r-r_m)]-2\exp[\xi(r-r_m)]\} \quad r_2 \leqslant r \leqslant r_3 \tag{3}$$

$$= \varepsilon(B_1+(r/r_m-r_3/r_m)\{B_2 + (r/r_m-r_4/r_m)[B_3+(r/r_m-r_3/r_m)B_4]\}), r_3 \leqslant r \leqslant r_4 \tag{4}$$

$$= \varepsilon\left(-\frac{C_6}{(r/r_m)^6}-\frac{C_8}{(r/r_m)^8}\right) \quad r \geqslant r_4 \tag{5}$$

where ε is the potential depth, r_m is the distance at the minimum potential and C_6 and C_8 are fitting parameters.

The parameters of the spline parts of the potential (a_1, a_2, a_3, a_4, b_1, b_2, b_3 and b_4) are completely determined by the continuity on the value and slope of the potential at r_1, r_2, r_3 and r_4.

Even at the present (ESMSV) level, there are eleven free parameters (ε, A_0, B_0, r_m, ξ, r_1, r_2, r_3, r_4, C_6 and C_8) which are far too many to determine from the present data. Accordingly we proceeded as follows: the long-range dispersion coefficients C_6 and C_8 were fixed at the values given by Fowler et al. [27] for CH_4–He, –Ne, –Ar and at the values given by Dunlop and Bignell [17] for CH_4–Kr, –Xe, leaving only nine parameters ε, A_0, B_0, r_m, ξ, r_1, r_2, r_3 and r_4 that were varied to fit the viscosity, diffusion data, isotopic thermal factors and thermal conductivity. This fitting is further supported by calculating the interaction second pressure virial coefficients and scattering cross-section data. Calculations were speeded by determining rough values of these parameters and then final convergence was obtained by iteration with the full isotropic potential. This decision leads to potential parameters of Table 1 as our best estimate of the CH_4–inert gas mixtures intermolecular potentials.

Analysis of traditional transport properties

The first check on the proposed potentials is to compare the transport properties i.e. viscosity (η), thermal conductivity (λ), self diffusion coefficient (D) and isotopic thermal factor (Iso) at different temperatures for CH_4–inert gas which are deduced using the formulas of Monchick et al. [28] and compared with the accurate experimental results of Kestin and

Table 1 Parameters of the trial potentials and the associated values of δ^a.

Potential parameters	CH_4–He	CH_4–Ne	CH_4–Ar	CH_4–Kr	CH_4–Xe
ε (K)/k_B	25.0	64.0	170.0	197.0	227.5
σ (nm)	0.333963	0.337244	0.344628	0.362329	0.38046
r_m (nm)	0.374	0.3775	0.385	0.404	0.424
ξ	6.475	6.50	6.61	6.72	6.75
A_0	0.00315	0.0035	0.0041	0.0045	0.011
B_0	20.6822	21.5175	19.15375	18.18	20.99648
r_1 (nm)	0.1575214	0.16	0.14	0.135	0.15
r_2 (nm)	0.230	0.2405	0.2359	0.25	0.3
r_3 (nm)	0.4441412	0.4077	0.440825	0.418342	0.4402
r_4 (nm)	0.6545	0.5983375	0.59675	0.56964	0.65
δ_η	0.45	0.61	0.39	0.54	0.68
δ_D	0.43	0.68	0.78	0.83	0.88
δ_{Iso}	0.9	0.99	0.85	0.81	0.92
δ_λ	–	–	0.67	–	–
δ_B	0.1	0.09	0.53	0.6	0.73
δ_{SC}	–	0.72	0.63	0.99	0.75
δ_t	0.55	0.71	0.66	0.77	0.8

δ^a is defined by $\delta^a = \sqrt{(1/N)\sum_{j=1}^{N}(1/n_J\sum_{j=1}^{n_j}\Delta_{ji}^{-2}(P_{ji}-p_{ji})^2)}$, where P_{ji} and p_{ji} are, respectively, the calculated and experimental values of property j at point i and Δ_{ji} is the experimental uncertainty of property j at point i. The subscripts η, D, Iso, λ, B, SC and t refer, respectively, to the viscosity, diffusion, isotopic thermal factor, thermal conductivity, pressure virial coefficient, integral scattering cross-section and total.

Ro [16], Dunlop and Bignell [17], Trengove et al. [18] and Zarkova et al. [19]. The agreement is excellent in the whole temperature range.

Analysis of the pressure second virial coefficient

The pressure second virial coefficient B at temperature T was calculated classically from [29]:

$$B(T) = 2\pi N_o \int_0^\infty [1 - \exp(-V(r)/k_B T)] r^2 dr \tag{6}$$

where N_o is the Avogadro number. The calculated $B(T)$ with the first three quantum corrections using the present ESMSV and other potentials [17,30,31] were compared with the experimental results [19–24] for CH_4–inert gas mixtures. The comparison is as shown in Fig. 1 for CH_4–Ar.

Analysis of integral scattering cross-sections

In the atom–atom interaction it is well known that the glory pattern contains detailed information on the potential well features, while the absolute value of the cross-section contains information about the long-range attraction. The experimental cross-sections [25] are compared with the results from calculations performed with the ESMSV of Table 1 in case of CH_4–Xe. From this comparison it can be seen that this potential yields good agreement with the experiment and better fitting to the glory extrema velocity locations.

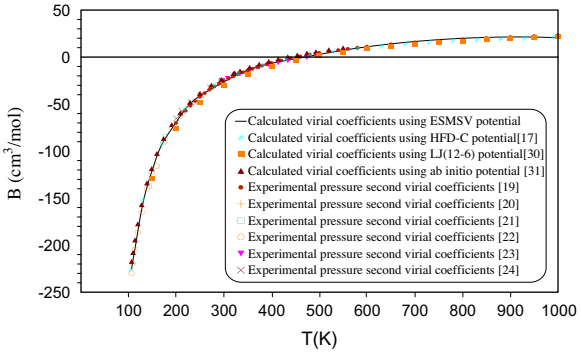

Fig. 1 CH_4–Ar second pressure virial coefficients in cm^3/mole vs. temperature in K using ESMSV potential with the parameters given in Table 1 and different literature potentials.

Theory of lineshapes

In this section the quantum mechanical calculations for collision-induced absorption (CIA) and for collision-induced light scattering (CILS) are described. The atomic wavefunctions, which enter the computation of the matrix elements, are obtained by numerical integration of the radial Schrödinger equation [10] using the energy density normalization.

Collision-induced absorption

Collision-induced absorption spectra (CIA) can be computed from quantum mechanical theory if the interaction potential is known along with a suitable model of the collision-induced dipole moment [8,32]. The absorption coefficient $\alpha(\omega, T)$ is related to the product of volume V and the so-called spectral function, $G(\omega, T)$, according to [10]

$$\alpha(\omega; T) = \frac{4\pi^2}{3\hbar c} n_1 n_2 \omega (1 - \exp(-\hbar\omega/k_B T)) G(\omega; T) \tag{7}$$

Here, ω designates angular frequency; $\hbar$ is Planck's constant; c is the speed of light in vacuum and n_1, n_2 is the number densities of the gases.

The spectral density $G(\omega, T)$ is defined in terms of the matrix elements of the isotropic overlap induction $\Lambda = 0$, induced electric octopole $\Lambda = 3$ and hexadecapole $\Lambda = 4$ as

$$G(\omega; T) = \sum_{\Lambda=0,3,4} \sum_{j,j'} \rho_{jj'}^{(\Lambda)} \frac{(2j+1)(2j'+1)}{(2\Lambda+1)} g_{L\Lambda}(\omega - \omega_{jj'}), \tag{8}$$

with the different coefficients which are defined in detailed in [32].

The spectral density $g_{L\Lambda}(\omega, T)$ is defined in terms of the matrix elements of the induced electric dipole moment $B_\Lambda(L; r)$ and Clebsch–Gordan coefficients $C(\lambda_1\lambda_2\Lambda; M_1M_2M_\Lambda)$ as

$$g_{L\Lambda}(\omega; T) = \lambda_o^3\hbar\sum_{l,l'}(2l+1)C(lLl'; 000)^2\omega(ll'j_1j_1'j_2j_2') \times\left(\int_0^\infty \exp(-E_l/k_BT)dE_l|\langle l, E_l|B_\Lambda(L; r)|l', E_l+\hbar\omega\rangle|^2 + \sum_{v,v'}\exp(-E_{vl}/k_BT)|\langle l, E_{vl}|B_\Lambda(L; r)|l', E_{v'l'}\rangle|^2\delta(E_{v'l'}-E_{vl}-\hbar\omega) + \sum_{v}\exp(-E_{vl}/k_BT)|\langle l, E_{vl}|B_\Lambda(L; r)|l', E_{vl}+\hbar\omega\rangle|^2 + \sum_{v'}\exp(-(E_{v'l'}-\hbar\omega)/k_BT)|\langle l, E_{v'l'}-\hbar\omega|B_\Lambda(L; r)|l', E_{v'l'}\rangle|^2\right) \quad (9)$$

where the first term in the right-hand side of Eq. (9), the integral, represents the free-free transitions of the collisional pair and is usually the dominant term in this expression. The second term, a sum, gives the bound–bound transitions of the van der Waals dimers with the vibrational and rotational quantum numbers n and l respectively. The last two terms account for bound-free and free-bound transitions of the molecular pair with the positive free-state energies, i.e. $E_l+\hbar\omega > 0$ and $E_{l'}-\hbar\omega$.

Spectral moments are defined as

$$M_n(T; \lambda_1\lambda_2L\Lambda) = \int_{-\infty}^{\infty}\omega^n G(\omega; T)d\omega \quad (10)$$

for $n = 0, 1, 2, \ldots$. These moments can be compared to values calculated directly from the sum rules [33].

It is often inconvenient to use tabular data in spectral moments and line shape computations. We have therefore, obtained an analytical models for the overlap ($L = 1$, $\Lambda = 0$), the octopole ($L = 4$, $\Lambda = 3$) and hexadecapole ($L = 5$, $\Lambda = 4$) contributions in the range of interest (near 5.98 Bohr) by a least mean squares fit. The different forms of these contributions are

$$B_0(L; r) = \mu_o\exp(-(r-\sigma)/r_o) \quad (11)$$

$$B_\Lambda(L; r) = \sqrt{(\Lambda+1)}\alpha Q_\Lambda/r^{L+1} \quad (12)$$

Here, $\alpha = 1.384$ a.u. [34] and $\alpha = 11.3304633$ a.u. [35] are the dipole polarizability of helium and argon respectively. $Q_3 = 3.96439$ a.u. [36] and $Q_4 = 10.723$ a.u. [36] are the octopole and hexadecapole moments of methane.

As a first step, we used the induced dipole, Eqs. (11) and (12) with the parameters given in Taylor and Borysow [32]. The crossed line in Fig. 2 gives the calculated line shape for comparison with the measurement at $T = 150$ K [32] for CH_4–He. The agreement is less than perfect. The calculated absorption is too weak and the high frequency wing is not well represented at all, in spite of the fact that the lowest three spectral moments of the measurements agree very closely with those of the computed line shape. Therefore, we add an overlap parts to the dispersion for octopole and hexadecapole contributions,

$$B_\Lambda(L; r) = \sqrt{(\Lambda+1)}\alpha Q_\Lambda/r^{L+1} + \mu_\Lambda\exp(-(r-\sigma)/r_\Lambda) \quad (13)$$

where μ_Λ are the dipole strengths at the root σ of the potential, $V(r) = 0$ at $r = \sigma$ and r_Λ are the ranges of the induced dipole. Ranges and strengths are the parameters determined by the analysis, with the results are given in Table 2.

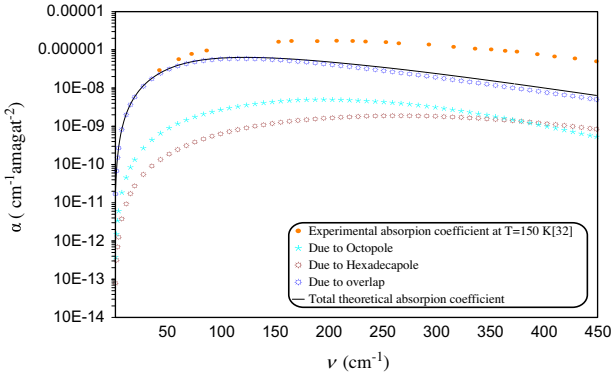

Fig. 2 Comparison between the calculated rototranslational collision-induced absorption spectrum of CH_4–He at $T = 150$ K using the present ESMSV potential given in Table 1 and induced dipole moment Eqs. (11) and (12) with the experimental one.

Table 2 Parameters of the dipole moment expansion coefficients defined in Eqs.(11) and (13).

Term $L\Lambda$	μ_Λ(a.u.)		r_Λ(a.u.)	
	CH_4–He	CH_4–Ar	CH_4–He	CH_4–Ar
10	0.00323	0.00375	0.70392	0.70865
43	0.00255	0.0105	0.6992	0.2551
54	0.00116	0.0035	0.62361	0.6142

Since an accurate determination of these spectral integrals requires knowledge of the absorption coefficient $\alpha(\omega, T)$ at low and high frequencies, which are not available, it is best to approximate the spectral function $G(\omega, T)$ by a three-parameter analytical model profile, the so-called BC model [37]. This model was chosen to provide a remarkably close representation of virtually all line shapes arising from exchange and dispersion force induction. These parameters have been determined by fitting the experimental spectrum, using a least mean squares procedure. The parameters of the fit are collected in Table 2 and the three lowest spectral moments of the measurements at different temperatures for CH_4–He [32] and at $T = 87$ K for CH_4–Ar [38] for each contribution are readily obtained. They are given in Table 3, and the absorption spectra are shown in Figs. 3 and 4.

The spectral lineshapes of scattering

At moderate densities, the CILS spectra are determined by binary interactions. It consists of purely translational scattering which includes scattering due to free pairs and bound dimers, and the other is due to the induced rotational scattering. The pair polarizability anisotropy giving rise to the translational scattering of the anisotropic light spectrum in the case of inert gases and spherical top molecules mixtures is given by the following formula [39].

$$\beta(r) = \frac{6\alpha_1\alpha_2}{r^3} + \frac{\left(3\alpha_1^2\alpha_2 + 3\alpha_2^2\alpha_1 + C_6\left(\frac{\gamma_1}{3\alpha_1}+\frac{\gamma_2}{3\alpha_2}\right)\right)}{r^6} + \frac{12\left(\alpha_1^2C_2+\alpha_2^2C_1\right)}{r^8} - g_o\exp\left(-\frac{r-\sigma}{r_o}\right) \quad (14)$$

Table 3 Translational spectral moments of absorption from different contributions of CH_4–He and CH_4–Ar using our empirical ESMSV potential.

$B_A(L;r)T(\mathrm{K})$	M_0*10^{62}(erg cm^6) Calculated	M_1*10^{50}(erg cm^6/s) Calculated	M_2*10^{36}(erg cm^6/s^2) Calculated
CH_4–He			
150 B_{10}	1.1334	8.35	4.391
150 B_{43}	1.095	8.92	4.78
150 B_{54}	0.0954	1.418	0.832
293 B_{10}	2.08	15.37	13.88
293 B_{43}	1.9	16.34	14.96
293 B_{54}	0.2125	3.102	3.01
353 B_{10}	2.51	18.55	19.7
353 B_{43}	2.263	19.7	21.2
353 B_{54}	0.27	3.93	4.404
CH_4–Ar			
87 B_{10}	1.201	2.422	0.678
87 B_{43}	14.28	86.68	25.42
87 B_{54}	0.1584	0.564	0.179

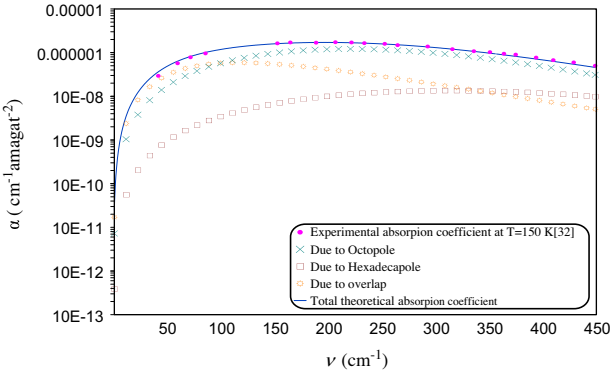

Fig. 3 Comparison between the calculated rototranslational collision-induced absorption spectrum of CH_4–He at $T = 150$ K using the present ESMSV potential given in Table 1 and induced dipole moment Eqs. (11) and (13) with the experimental one.

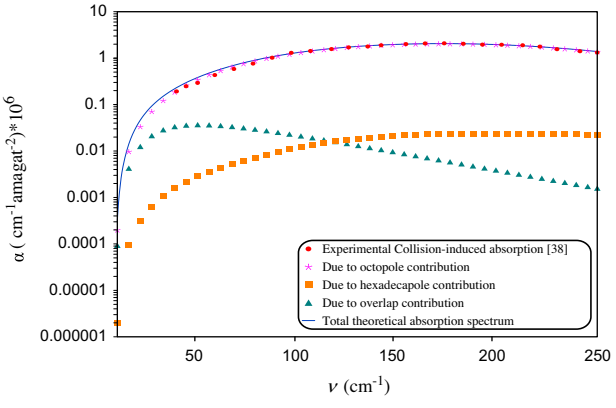

Fig. 4 Comparison between the calculated rototranslational collision-induced absorption spectrum of CH_4–Ar at $T = 87$ K using the present ESMSV potential given in Table 1 and induced dipole moment Eqs. (11) and (13) with the experimental one.

where α, γ and C are the dipole, hyperpolarizability and quadrupole polarizability with the label 1 refers to CH_4 and 2 refers to Ar or Xe. Values of the polarizabilities used in Eq. (14) are given in Table 4.

A purely long-range interaction mechanism, involving the participation of high order polarizabilities, has been invoked to account for induced rotational scattering [8,44]. Contributions from the dipole–quadrupole (**A**) and dipole–octopole (**E**) polarizabilities for CH_4 symmetry give the intensity of the observed rotational spectra with the predictions of the mean square polarizability models in the case of the isotropic and anisotropic spectra as

$$\langle \alpha_{xz}^2 \rangle = \frac{12}{5}(\alpha_1\alpha_2)^2 r^{-6} + \frac{48}{35}\left((\alpha_2\mathbf{A}_1)^2\right) r^{-8} + \frac{11}{9}\left((\alpha_2\mathbf{E}_1)^2\right) r^{-10} + \cdots \quad (15)$$

The angular brackets $\langle \ldots \rangle$ denote an average over all orientations of the intermolecular and molecular axes.

The various terms in Eq. (15) give rise to the following selection rules on J the total angular momentum quantum number:

$$\begin{aligned}
&\alpha_i\mathbf{A}_j, \quad \Delta J_i = 0, \quad \Delta J_j = 0, \pm1, \pm2, \pm3, \quad J_j + J_j' \geqslant 3\\
&\alpha_i\mathbf{E}_j, \quad \Delta J_i = 0, \quad \Delta J_j = 0, \pm1, \pm2, \pm3, \pm4, \quad J_j + J_j' \geqslant 4,\\
&\mathbf{A}_i\mathbf{A}_j, \quad \Delta J_i = 0, \pm1, \pm2, \pm3, \quad \Delta J_j = 0, \pm1, \pm2, \pm3,\\
&\qquad\qquad J_i + J_i' \geqslant 3, \quad J_j + J_j' \geqslant 3\\
&\mathbf{A}_i\mathbf{E}_j, \quad \Delta J_i = 0, \pm1, \pm2, \pm3, \quad \Delta J_j = 0, \pm1, \pm2, \pm3, \pm4,\\
&\qquad\qquad J_i + J_i' \geqslant 3, \quad J_j + J_j' \geqslant 4,\\
&\mathbf{E}_i\mathbf{E}_j, \quad \Delta J_i = 0, \pm1, \pm2, \pm3, \pm4, \quad \Delta J_j = 0, \pm1, \pm2, \pm3, \pm4,\\
&\qquad\qquad J_i + J_i' \geqslant 4, \quad J_j + J_j' \geqslant 4,
\end{aligned}$$

The quantum theory is applied for the accurate computation of the CILS absolute translational intensities of the methane pairs. Numerically, this is done by means of the propagative two-point Fox-Goodwin integrator [45,46], where the ratio of the wavefunction, defined at adjacent points on a spatial grid, is built step-by-step.

As regards our problem, binary anisotropic light scattering spectrum is computed quantum–mechanically, as a function of frequency shifts ν, at temperature T by using the expressions [47–49]:

$$I_{\mathrm{aniso}}(\nu) = \frac{2}{15} hc\lambda^3 k_s^4 \sum_{J=0,J\mathrm{even}}^{J_{\max}} g_J b_J^{J'} (2J+1) \times \int_0^{E_{\max}} |\langle \psi_{E',J'} | \beta | \psi_{E,J} \rangle|^2 \exp\left(\frac{-E}{k_B T}\right) dE \quad (16)$$

The symbol k_s stands for the Stokes wave number of the scattered light, h is Planck's constant and c is the speed of the light. Constant λ account for the thermal de Broglie wavelength, $\lambda = h/\sqrt{2\pi\mu k_B T}$, with μ the reduced mass of methane and argon or xenon and k_B Boltzmann's constant. Symbol $\psi_{E,J}$ designates the scattering wave function and $E_{\max}$ the maximum value of the energy that is required to obtain convergence of the integrals.

In this expressions, $\beta = \beta(r)$ denote the anisotropy of the quasimolecule, g_J the nuclear statistical weight and $b_J^{J'}$ are intensity factors involving the rotational quantum numbers J and J' of the initial and final states, respectively.

Table 4 Parameters of Eq. (14) used in calculations.

	CH_4	Ar	Xe	CH_4–Ar	CH_4–Xe
α (a.u.)	17.828 [40]	11.3304633 [35]	27.0514 [43]	–	–
γ (a.u.)	3079.2 [41]	1170.735 [42]	7889.9375 [43]	–	–
C (a.u.)	60.45 [41]	50.21 [35]	211.053 [43]	–	–
g_o (a.u.)	–	–	–	1.01225	1.2147
r_o (a.u.)	–	–	–	0.85605	0.94486

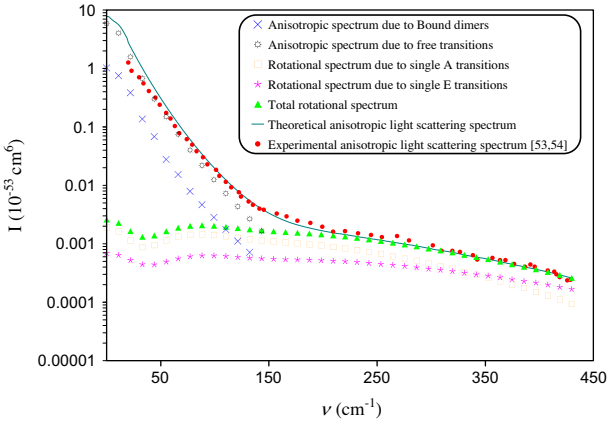

Fig. 5 Total anisotropic collision-induced light scattering spectrum of CH_4–Ar at $T = 295$ K using the isotropic ESMSV potential given in Table 1.

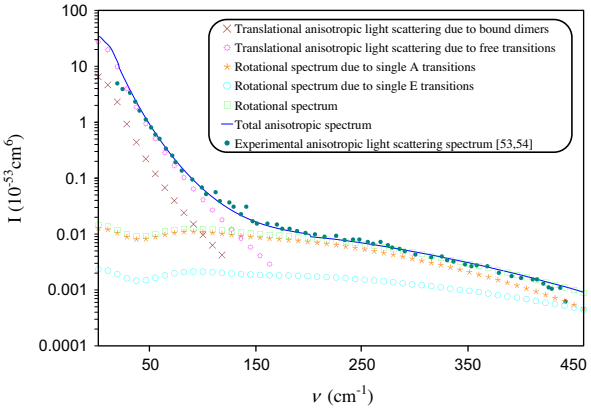

Fig. 6 Total anisotropic collision-induced light scattering spectrum of CH_4–Xe at $T = 295$ K using the isotropic ESMSV potential given in Table 1.

The total theoretical intensities of the anisotropic light scattering spectrum are the sum of the translational spectra due to the transitions of bound–bound, bound–free and free–free states and rotational spectrum.

With the spectral intensities $I_{\text{aniso}}(\nu)$ in cm^6 as input and through the following analytical expression we are able to deduce the experimental anisotropic moments [50]

$$M_{2n}^{\text{aniso}} = \frac{15}{2}\left(\frac{\lambda_o}{2\pi}\right)^4 \int_{-\infty}^{\infty} (2\pi c\nu)^{2n} I_{\text{aniso}}(\nu)\, d\nu \tag{17}$$

These moments can be compared to values calculated directly from the sum rules with the quantum corrections [51].

In order to calculate the line profiles and the associated moments, the intermolecular potential and the anisotropy models are needed. Results with dipole-induced-dipole (DID) [52] and corrected dipole-induced-dipole (C.DID) [53] polarizability models can be compared with experiment [53,54] to assess the quality of our empirical potential and anisotropy models.

Comparisons between the calculations and experiments [53,54] are shown in Figs. 5 and 6 for the intensities of the anisotropic light scattering spectra at room temperatures for methane mixtures with argon and xenon.

Concerning the multipolar contributions of single **A** and single **E** transitions, different values of the dynamic independent tensor components **A** and **E** may be used to fit the experimental anisotropic intensities in the frequency ranges (75–450) cm^{-1} for CH_4–inert gas mixtures. Figs. 5 and 6 suggest that there are a choices of **A** and **E** for which the theoretical and experimental anisotropic spectra [53,54] fit the best $|\mathbf{A}| = 0.74$ Å^4 and $|\mathbf{E}| = 2.47$ Å^5 for CH_4–CH_4 using our empirical ESMSV intermolecular potential. These coefficients of multipolar polarizabilities are in good agreement with the experimental values of Shelton and Tabisz [55].

Conclusion

We have adopted a models for the dipole moment $\mu(r)$ and pair polarizability $\beta(r)$ with adjustable parameters for each, which we determined by fitting to the spectral profiles for absorption and scattering using quantum mechanics and to the first three moments of the measured absorption spectrum and anisotropic light scattering spectra using methods of classical mechanics with quantum corrections [33].

The present study further demonstrates that the empirical ESMSV potential models, with the parameters fitted to the different transport and thermophysical properties beside to the integral scattering cross-sections are a very good representation of the intermolecular potential of gaseous CH_4–inert gas mixtures. The profiles of the two-body anisotropic collision-induced light scattering spectra at room temperature can be accounted for by a calculation employing a classical trajectory to simulate the collision. The significant contributions to the spectra by bound dimers are found to be essentially the same as that arrived at by a full quantum mechanical calculations. At high frequencies we show that most of the intensities may be attributed to multipolar contributions involving the dipole–quadrupole **A** and dipole–octopole **E** polarizability tensors. Moreover, the very broad frequency range provides enough information to deduce values for the independent components of **A** and **E**, this is confirmed by the good agreement between our fitted values from spectra and the one measured by Shelton and Tabisz [55]. Also for these mixtures, the

lineshape calculations for both induced pure translational and rotational scattering worked well at room temperature like CF_4–inert gases [44] with the well known electric properties of CF_4, but the spectra of CH_4–inert gases are spreading over larger frequency shifts.

References

[1] El-Kader MSA, Maroulis G, Bich E. Rototranslational collision-induced absorption and collision-induced light scattering spectra of molecular hydrogen using isotropic intermolecular potentials. Chem Phys 2012;403:37–51.

[2] El-Kader MSA. Collision-induced absorption (CIA) spectra and ground-state potentials of inert gas mixtures. J Quant Spectrosc Radiat Transfer 2011;112:1533–42.

[3] El-Kader MSA, Bancewicz T. Lineshapes of collision-induced absorption (CIA) and of collision-induced scattering (CIS) for monatomic gas mixtures of Ne–Ar. Mol Phys 2011;109:457–66.

[4] El-Kader MSA, Maroulis G. An empirical multi-parameter anisotropic intermolecular potential, collision-induced absorption and predicted collision-induced light scattering spectra for CF_4–He. Chem Phys 2011;388:78–85.

[5] Kiss ZJ, Welsh HL. Pressure-induced infrared absorption of mixtures of rare gases. Phys Rev Lett 1959;2:166–73.

[6] Buontempo U, Cunsolo S, Jacucci G. Translational spectrum of the liquid A–Ne solution. Phys Lett A 1970;31:128–36.

[7] Tabisz GC, Mol. Specialist periodical reports, the chemical societies, London. Mol Spectrosc 1979;6:136.

[8] Frommhold L. Collision-induced scattering of light and the diatom polarizabilities. Adv Chem Phys 1981;46:1–72.

[9] Bafile U, Magli R, Barocchi F, Zoppi M, Frommhold L. Line shape and moment analysis in depolarized induced light scattering. Mol Phys 1983;49:1149–66.

[10] El-Kader MSA. Collision-induced light scattering spectra and pair-polarizability trace and anisotropy of gaseous neon. Phys Lett A 2009;373:243–51.

[11] El-Kader MSA, El-Sadek AA, Taher BM, Maroulis G. Empirical pair polarizability anisotropy and interatomic potential for monatomic gas mixture of Kr and Xe. Mol Phys 2011;109:1677–89.

[12] El-Kader MSA, El-Sheikh SM, Bancewicz T, Hellmann R. Contributions of multipolar polarizabilities to the isotropic and anisotropic light scattering induced by molecular interactions in gaseous methane. J Chem Phys 2009;131:044314.

[13] Maitland GC, Wakeham WA. Direct determination of intermolecular potentials from gaseous transport coefficients alone. Part II. Application to unlike monatomic interactions. Mol Phys 1978;35:1443–69.

[14] Maitland GC, Rigby M, Smith EB, Wakeham WA. Intermolecular forces—their origin and determination. Oxford: Clarendon; 1981.

[15] Buck U, Schleusener J, Malika DJ, Secrest D. On the argon–methane interaction from scattering data. J Chem Phys 1981;74:1707–17.

[16] Kestin J, Ro ST. Transport properties of nine binary and two ternary mixtures of gases at low density. Ber BunsenGes 1976;80:619–24.

[17] Dunlop PJ, Bignell CM. Diffusion and thermal diffusion in binary mixtures of methane with noble gases and of argon with krypton. Physica A 1987;145:584–96.

[18] Trengove RD, Robjohns HL, Dunlop PJ. Diffusion coefficients and thermal diffusion factors for five binary systems of methane with the noble gases. Ber Bunsenges Phys Chem 1982;86:951–5.

[19] Zarkova L, Hohm U, Damyanova M. Viscosity and pVT–second virial coefficient of binary noble–globular gas and globular–globular gas mixtures calculated by means of an isotropic temperature-dependent potential. J Phys Chem Ref Data 2003;32:1591–705.

[20] Martin ML, Trengove RD, Harris KR, Dunlop PJ. Excess second virial coefficients for some binary gas mixtures. Aust J Chem 1982;35:1525–9.

[21] Thomaes G, van Steenwinkel R, Stone W. The second virial coefficient of two gas mixtures. Mol Phys 1962;5:301–6.

[22] Byrne MA, Jones MR, Staveley LAK. Trans Faraday Soc 1968;64:1747.

[23] Strein K, Lichtenthaler RN, Schramm B, Schafer K. Ber Bunsenges Phys Chem 1971;75:1308.

[24] Hahn R, Schäfer K, Schramm B. II. Messungen zweiter Virialkoeffizienten im Temperaturbereich von 200–300 K. Ber Bunsenges Phys Chem 1974;78:287–9.

[25] Liuit G, Pirani F, Buck U, Schmidt B. Methane–rare gas interaction potentials from scattering experiments. Chem Phys 1988;126:1–6.

[26] Farrar JM, Lee YT. Intermolecular potentials from crossed beam differential elastic scattering measurements. V. The attractive well of He_2. J Chem Phys 1972;56:5801–7.

[27] Fowler PW, Lazzeretti P, Zanasi R. The second virial coefficient of two gas mixtures. Mol Phys 1989;68:853–65.

[28] Monchick L, Yun KS, Mason EA. Formal kinetic theory of transport phenomena in polyatomic gas mixtures. J Chem Phys 1963;39:654–69.

[29] Dymond JH, Smith EB. The virial coefficients of pure gases and mixtures. Oxford: Oxford University; 1980.

[30] Bellm J, Reineke W, Schäfer K, Schramm B. I. Messungen zweiter Virialkoeffizienten im Temperaturbereich von 300–550 K. Ber Bunsenges Phys Chem 1974;78:282–6.

[31] Heijmen TGA, Korona T, Moszynski R, Wormer PES, Avoird A. *Ab initio* potential-energy surface and rotationally inelastic integral cross sections of the Ar–CH_4 complex. J Chem Phys 1997;107:902–13.

[32] Taylor RH, Borysow A, Frommhold L. Concerning the rototranslational absorption spectra of He–CH, pairs. J Mol Spectrosc 1988;129:45–58.

[33] Moraldi M, Borysow A, Frommhold L. Quantum sum formulae for the collision-induced spectroscopies: molecular systems as H_2–H_2. Chem Phys 1984;86:339–47.

[34] Dalgarno A, Kingston AE. Proc R Soc London Ser A 1960;259:424.

[35] Maroulis G. Computational aspects of interaction hyperpolarizability calculations. A study on H_2–H_2, Ne–HF, Ne–FH, He–He, Ne–Ne, Ar–Ar and Kr–Kr. J Phys Chem A 2000;104:4772–9.

[36] Amos RD. An accurate *ab initio* study of the multipole moments and polarizabilities of methane. Mol Phys 1979;38:33–45.

[37] Borysow A, Frommhold L. In: Birnbaum G, editor. Phenomena induced by intermolecular interactions. New York: Plenum; 1985, p. 67.

[38] Marabella L, Ewing GE. Collision induced far infrared absorption of solutions of CH_4 and CD_4 in liquid argon. J Chem Phys 1972;56:5445–52.

[39] El-Sheikh SM, Tabisz GC, Buckingham AD. Collision-induced light scattering by isotropic molecules: the role of the quadrupole polarizability. Chem Phys 1999;247:407–12.

[40] Meinander N, Tabisz GC, Zoppi M. Moment analysis in depolarized light scattering: Determination of a single-parameter empirical pair polarizability anisotropy for Ne, Ar, Kr, Xe And CH_4. J Chem Phys 1989;84:3005–13.

[41] Maroulis G. Electric dipole hyperpolarizability and quadrupole polarizability of methane from finite-field coupled cluster and fourth-order many-body perturbation theory calculations. Chem Phys Lett 1994;226:420–6.

[42] Buckingham AD, Clarke KL. Long-range effects of molecular interactions on the polarizability of atoms. Chem Phys Lett 1978;57:321–5.

[43] Maroulis G, Haskopoulos A, Xenides D. New basis sets for xenon and the interaction polarizability of two xenon atoms. Chem Phys Lett 2004;396:59–64.
[44] El-Kader MSA, Bancewicz T, Maroulis G. Higher order multipolar polarizabilities of carbon tetrafluoride from isotropic and anisotropic light scattering experiments. J Mol Struct 2010;984:262–7.
[45] Norcross DW, Seaton MJ. Asymptotic solutions of the coupled equations of electron-atom collision theory for the case of some channels closed. J Phys B 1973;6:614–21.
[46] Chrysos M, Lefebvre R. Resonance quantization with persistent effects. J Phys B 1993;26:2627–47.
[47] Gaye O, Chrysos M, Teboul V, Le Duff Y. Trace polarizability spectra from Ar_2 quasimolecules in collision-induced scattering. Phys Rev A 1997;55:3484–90.
[48] Chrysos M, Gaye O, Le Duff Y. Quantum description of high-frequency Raman scattering from pairs of argon atoms. J Phys B 1996;29:583–93.
[49] Chrysos M, Gaye O, Le Duff Y. Orientational correlation functions and polarization selectivity for nonlinear spectroscopy of isotropic media. I. Third order. J Chem Phys 1996;105: 1–12.
[50] Barocchi F, Guasti A, Zoppi M, El-Sheikh SM, Tabisz GC, Meinander N. Temperature dependence of the collision-induced light scattering by CH_4 gas. Phys Rev A 1989;39:4537–44.
[51] Nienhuis G. On the theory of quantum corrections to the equations of state and to the particle-distribution functions. J Math Phys 1970;11:239–43.
[52] Silberstein L. Molecular refractivity and atomic interaction. Philos Mag 1917;33:521–33.
[53] Meinander N, Penner AR, Bafile U, Barocchi F, Zoppi M, Shelton DP, Tabisz GC. The spectral profile of the collision-induced translational light scattering by gaseous CH_4. Mol Phys 1985;54:493–503.
[54] Penner AR, Meinander N, Tabisz GC. The spectral intensity of the collision-induced rotational Raman scattering by gaseous CH_4 and CH_4–inert gas mixtures. Mol Phys 1985;54:479–92.
[55] Shelton DP, Tabisz GC. Binary collision-induced light scattering by isotropic molecular gases. Mol Phys 1980;40:299–308.